ACS OMEGA

http://pubs.acs.org/journal/acsodf

Article

Azo-Linked Porous Organic Polymers for Selective Carbon Dioxide Capture and Metal Ion Removal

Mahmoud M. Abdelnaby,* Tawfik A. Saleh, Mostafa Zeama, Mahmoud Atef Abdalla, Hossam M. Ahmed, and Mohamed A. Habib

Cite This: *ACS Omega* 2022, 7, 14535−14543

Read Online

ACCESS | Metrics & More | Article Recommendations | Supporting Information

ABSTRACT: The facile and environmentally friendly synthesis of porous organic polymers with designed polar functionalities decorating the interior frameworks as an excellent adsorbent for selective carbon dioxide capture and metal ion removal is a target worth pursuing for environmental applications. In this regard, two azo-linked porous organic polymers denoted man-Azo-P1 and man-Azo-P2 were synthesized in water by the azo-linking of 4,4′-diaminobiphenyl (benzidine) and 4,4′-methylenedianiline, respectively, with 1,3,5-trihydroxybenzene. The resulting polymers showed good BET surface areas of 290 and 78 $m^2\ g^{-1}$ for man-Azo-P1 and man-Azo-P2, respectively. Due to the enriched core functionality of the azo (−N═N−) and hydroxyl groups along with the porous frameworks, man-Azo-P1 exhibited a good CO_2 uptake capacity of 32 $cm^3\ g^{-1}$ at 273 K and 1 bar, in addition to the remarkable removal of lead (Pd), chromium (Cr), arsenic (As), nickel (Ni), copper (Cu), and mercury (Hg) ions. This performance of the synthesized man-Azo-P1 and man-Azo-P2 in the dual application of CO_2 capture and heavy metal ion removal highlights the unique properties of azo-linked POPs as excellent and stable sorbent materials for the current challenging environmental applications.

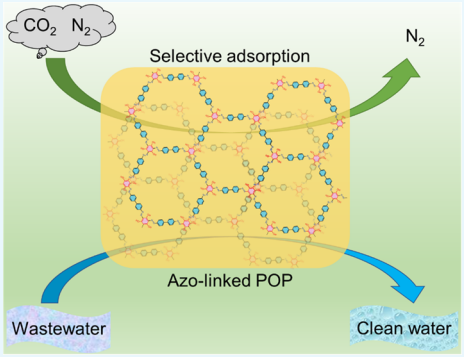

INTRODUCTION

The development of advanced porous materials has attracted tremendous and deep interest from both the academic and industrial scientific communities in various fields. Porous materials such as zeolites,[1] metal organic frameworks (MOFs),[2] covalent organic frameworks (COFs),[3] porous polymers,[4] and porous carbons[5,6] have increasingly shown great promise in different energy and environmental applications, including but not limited to catalysis, gas separation, CO_2 capture, and wastewater treatment. Porous organic polymers (POPs) have emerged as versatile solid adsorbents for selective CO_2 capture and metal ion removal due to their exceptional physical, chemical, and mechanical properties in addition to their high surface areas and structural diversity with the ability to introduce various functional groups. POPs are commonly constructed by robust covalent bonds, which make their robust porous structure a prominent porous sorbent candidate for efficient CO_2 capture.[7] On the other hand, the superior chemical stability of the POPs with the excellent ability to survive in the harsh environmental condition of water at different pHs makes them among the top candidates for the removal of toxic metal ions such as mercury (Hg), arsenic (As), chromium (Cr), copper (Cu), and nickel (Ni) from wastewater. These toxic metal ions are a serious problem for the environment as well as for human consumption.[8]

Researchers have devoted great effort to develop a wide range of functional porous organic polymers such as covalent organic frameworks (COFs),[3,9] covalent triazine frameworks (CTFs),[10,11] porous aromatic frameworks (PAFs),[12] conjugated microporous polymers (CMPs),[13,14] polymers with intrinsic microporosity (PIMs),[15,16] and hyper-cross-linked polymers (HCPs).[17−19] Despite the varieties of developed POPs, their large scale industrial implementation is still challenging due to the low yield and costly starting materials for the synthesis (e.g., COFs and CMPs), the expensive catalysts used (e.g., CMPs and PAFs), and the high synthesis temperature (e.g., PAFs and CTFs). Azo-linked POPs have recently attracted significant interest due to their facile, green synthesis at low temperature in water and high yield. The facile synthesis and diversity to introduce polar functional groups and Lewis basic sites (known to have good binding to CO_2 gas) pave the way for the azo-linked POPs to be efficient solid sorbents for CO_2 capture and metal ion removal from wastewater. The azo-linked POPs with nitrogen double bonds (N═N, azo bond) work as selective binding sites for

Received: October 21, 2021
Accepted: April 11, 2022
Published: April 21, 2022

https://doi.org/10.1021/acsomega.1c05905
ACS Omega 2022, 7, 14535−14543

Scheme 1. Synthesis of the Azo-Linked Polymers man-Azo-P1 (a) and man-Azo-P2 (b)

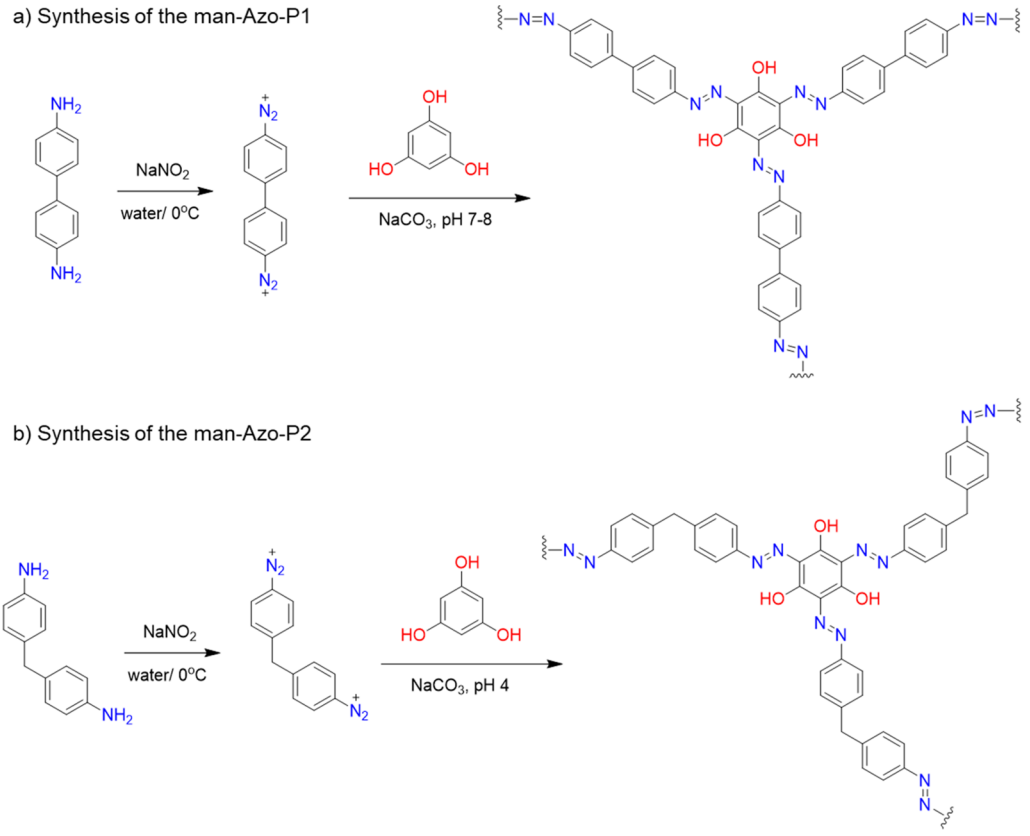

the CO_2 and metal ions without compromising the chemical stability.[20−23]

Here, we present the facile and green synthesis of azo-linked porous organic polymers bearing accessible polar phenolic and azo functional groups. The synthetic strategy of the novel azo polymers is based on the diazotization of aromatic diamines, typically 4,4′-diaminobiphenyl (benzidine) or 4,4′-methylenedianiline, and then coupling with the 1,3,5-trihydroxybenzene moiety in water (Scheme 1). The resulting frameworks were fully characterized, and their permanent porosity was proved. The CO_2 capture and CO_2/N_2 selectivity were studied for the azo-linked POPs. Furthermore, due to the designed chelating sites of these polymers, the selective removal of heavy-metal ions from wastewater was also investigated.

EXPERIMENTAL SECTION

Materials and General Techniques. All chemicals and reagents were used as received without further purification. Biphenyl (99% purity), 1,3,5-trihydroxybenzene (phloroglucinol, 98%), 4,4′-methylenedianiline (97% purity), sodium nitrite (98% purity), and sodium carbonate (98% purity) were purchased from Alfa Aesar. Nitric acid (70%), sulfuric acid (98%), hydrochloric acid (HCl, 37%), and toluene (high purity) were obtained from Acros. Methanol (99.9% purity), *N*,*N*′-dimethylformamide (DMF, 99% purity) and Pd/C (5% w/w) were purchased from Millipore Sigma. Ultrapure water was obtained using a Milli-Q Ultrapure instrument. For the metal removal analysis, standard solutions (1000 ppm) containing lead (Pb(II)), mercury (Hg(II)), arsenic (As(III)), copper (Cu(II)), chromium (Cr(III)), and nickel (Ni(II)) were purchased from Sigma-Aldrich and used to prepare the required solutions for testing with a predetermined initial concentration. For gas sorption analysis, nitrogen gas (99.999% purity), carbon dioxide gas (99.99% purity), and helium (99.999% purity) were supplied from Air Liquide, Dammam, Saudi Arabia.

Gas Sorption Measurements. Porosity and low-pressure gas uptake measurements were conducted using a Quantachrome Quadrasorp Evo volumetric analyzer. The samples were activated before the measurement by heating at 110 °C under reduced pressure (<50 mTorr). For the N_2 isotherms for the BET surface area calculation, liquid nitrogen was used, while for the gas uptake at 0 and 25 °C a water chiller circulator was used for cooling.

Metal Ion Removal Studies. Adsorption experiments were performed to evaluate the prepared materials for the removal of metal ions from aqueous media. The effect of the related experimental conditions such as adsorbent dosage, solution pH, and contact time was investigated at atmospheric temperature. Metal ion detection was performed in triplicate, and the average was considered to calculate the percent removal as

$$\text{adsorption}\ (\%) = \frac{C_i - C_f}{C_i} \times 100 \quad (1)$$

where the initial and final metal ions concentrations are C_i and C_f, respectively.

The capacities of adsorption were evaluated by the equation

$$q_t = (C_i - C_t) \times \frac{V}{m} \quad (2)$$

where C_t refers to the metal concentration at any time t, V represents the volume of metal solution (L), m denotes the

https://doi.org/10.1021/acsomega.1c05905
ACS Omega 2022, 7, 14535−14543

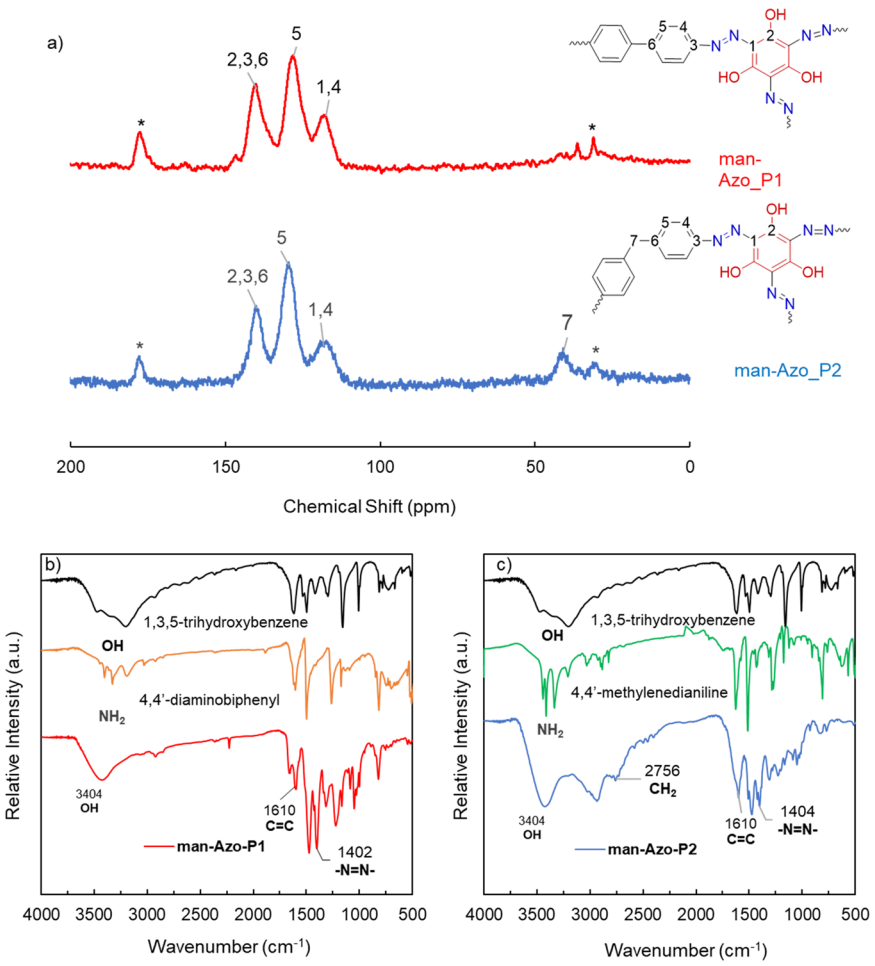

Figure 1. Structure characterization of the synthesized polymers: (a) CP-MAS ^{13}C NMR spectra with the corresponding peak assignments of FTIR spectra of (b) man-Azo-P1 (c) and man-Azo-P2 polymers and their corresponding monomers.

mass of the adsorbent (mg), and q_t refers to the adsorption capacity of the prepared polymer.

The developed polymers were subjected to a five-cycle adsorption/desorption test to estimate their reuse performance. After adsorption, the metals were desorbed from the polymers using 10 mL of 0.5 mol L^{-1} HCl. Thus, the adsorbent (polymer) was treated with HCl solution with stirring for 10 min to ensure all metals were desorbed from the polymer. The polymer was then separated from the solution and allowed to dry. It was then used for the adsorption in the next cycle.

Characterization Instruments. The high-resolution solid-state cross-polarization magic angle spinning ^{13}C nuclear magnetic resonance (CP-MAS ^{13}C NMR) spectra were obtained on a JEOL ECA-600 spectrometer (14.1 T) equipped with an additional 1 kW power amplifier. The pulse was set at 3.8 μs, and 10000 scans were accumulated with spinning at 15 kHz and a 5 s delay. A 4 mm ZrO_2 rotor was used. The chemical shifts were referenced to the carbon species of adamantane at 38.52 and 29.47 ppm. Fourier transform infrared (FT-IR) spectra were obtained on a PerkinElmer 16 PC spectrometer using KBr pellets. The spectra were recorded from 4000 to 500 cm^{-1}. The FT-IR signals were identified as follows: br, broad; s, strong; m, medium; w, weak. The SEM images and the elemental composition (C and N) contents of the polymers were determined from an EDX analysis using a Quattro S field-emission scanning electron microscope (FESEM). The thermal stability of the synthesized azo polymers was identified by a thermogravimetric analysis (TGA) using a TA Q500 instrument under an air flow with a heating rate of 10 °C/min. Powder X-ray diffraction (PXRD) was carried out using a Rigaku MiniFlex II instrument with Cu Kα radiation (λ = 1.541 Å). For the metal removal studies, a Plasma Quant PQ 9000 ICP-OES instrument was used to determine the metal contents.

Material Synthesis. According to previous literature, the synthesis of the 4,4′-diaminobiphenyl (benzidine) monomer was started by the nitration of biphenyl, and then the resulting 4,4′-dinitrobiphenyl was reduced using Pd/C in ethanol to produce high-purity 4,4′-diaminobiphenyl.[24] The syntheses of man-Azo-P1 and man-Azo-P2 were carried out by following the reported procedure[25] with some modifications. The coupling reaction to form the azo POPs was carried out through two *in situ* steps: first the formation of the diazonium salts and then coupling with hydroxybenzene.

Synthesis of man-Azo-P1. 4,4′-Diaminobiphenyl (9 mmol, 1.6 g) was suspended in 20 mL of DI water and concentrated HCl (4.2 mL) in a 100 mL round flask, and the mixture was stirred in an ice bath (0−5 °C) or 15 min; after that a precooled sodium nitrite solution (27 mmol, 1.95 g in 10 mL) was added dropwise. At this point, a clear solution of the diazonium salt was formed. The solution was stirred at 0 °C for 30 min and then neutralized to pH 7−8 using drops of a saturated $NaCO_3$ aqueous solution. In another 50 mL round

https://doi.org/10.1021/acsomega.1c05905
ACS Omega 2022, 7, 14535−14543

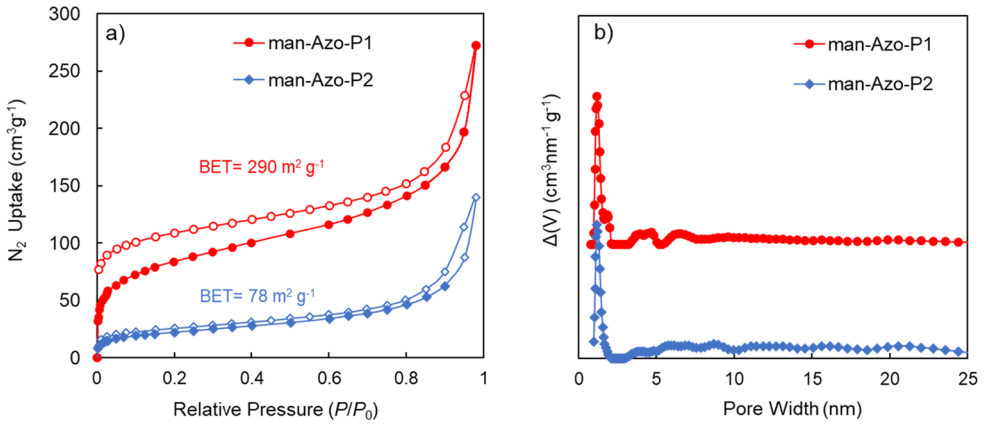

Figure 2. (a) N_2 sorption isotherms at 77 K for man-Azo-P1 (red, circles) and man-Azo-P2 (blue, rhombohedra). (b) Pore size distribution (PSD) of man-Azo-P1 (red) and man-Azo-P2 (blue). Filled and open markers represent the adsorption and desorption isotherms, respectively. Solid lines are used for clear visualization.

flask, a precooled solution of phloroglucinol (6 mmol, 0.67 g in 30 mL) was neutralized to pH 7−8 using drops of saturated $NaCO_3$ aqueous solution, which was subsequently added dropwise to the diazonium salt solution. The instantaneous precipitation of a dark brown polymer occurred with the addition. The reaction was then stirred for 12 h. The product was separated by filtration under reduced pressure and repeatedly washed with water and once with methanol and then washed with 30 mL of DMF with stirring for 2 h. After that, the product was filtered and subjected to Soxhlet extraction with methanol for 24 h. Finally, the product was dried in a vacuum oven (pressure less than 100 mTorr) at 75 for 12 h (1.45 g, 80% yield). Anal. Calcd for $C_{48}H_{32}N_{12}O_6$: C, 66.04; H, 3.69; N, 19.25. Found experimentally from the EDX analysis: C, 70.3; N, 12.7. FT-IR (KBr, cm^{-1}): 3404 (br), 1610 (m), 1402 (m), 1308 (w), 105 (w).

Synthesis of man-Azo-P2. man-Azo-P2 was synthesized by following the same procedure as for man-Azo-P1 except using 4,4′-methylenedianiline (9 mmol, 1.78 g) and adjustment of the pH to only 4 instead of 8 to produce a brown polymeric product (2.4 g, yield 98%). Anal. Calcd for $C_{48}H_{32}N_{12}O_6$: C, 66.95; H, 4.18; N, 18.37. Found experimentally from the EDX analysis: C, 21.7; N, 8.9. FT-IR (KBr, cm^{-1}): 3404 (br), 2756 (w), 1610 (m), 1402 (m), 1308 (w), 105 (w).

RESULTS AND DISCUSSION

Synthesis Strategy for the Azo-Linked Polymers man-Azo-P1 and man-Azo-P2. To realize the green and facile synthesis of robust N-rich POPs as solid sorbents that can work to solve practical energy and environmental challenges, we targeted the utilization of the azo-coupling reaction of aromatic diamines and phenolic moieties (Scheme 1). The resulting azo group (−N═N−) and the adjacent OH can lead to the selective binding of CO_2 and heavy-metal ions. Although several methods have been investigated for the azo-coupling reaction, our synthetic design and monomer selection were chosen to optimize the azo-coupling reaction in which the water is the solvent, and no temperature or expensive catalyst was required. We employed the diazotization of 4,4′-diaminobiphenyl and 4,4′-methylenedianiline using $NaNO_2$ and a catalytic amount of concentrated HCl in water at 0 °C. After that, coupling with the activated 1,3,5-trihydroxybenzene produces the respective highly cross-linked azo polymers man-Azo-P1 and man-Azo-P2. Subsequently, the resulting polymers were purified by filtration and washing with water, methanol, and DMF and then Soxhlet extraction by methanol to remove any inorganic salts and unreacted materials.

Structure Characterization. The successful formation of the azo-linked polymers was confirmed by the solid-state cross-polarization magic angle spinning (CP-MAS) ^{13}C NMR and the Fourier transform infrared (FT-IR) spectra (Figure 1). The characteristic CP-MAS ^{13}C NMR signals for the two monomer units constructing both man-Azo-P1 and man-Azo-P2 were assigned as follows (Figure 1a): (i) the peak at δ 117 ppm corresponds to aromatic carbons of the 1,3,5-trihydroxybenzene attached to the azo group (carbon 1, C_{ph}−N═N−).

In comparison, the peak at δ 140 ppm is assigned to the aromatic carbon attached to the OH group (carbon 2, C−OH). (ii) Peaks at δ 117, 128, and 140 ppm are characteristic of 4,4′-diaminobiphenyl and 4,4′-methylenedianiline aromatic carbons. (iii) δ 40 ppm is the characteristic peak for the methylene (−CH_2−) linkage of the 4,4′-methylenedianiline monomer of man-Azo-P2, which is not present in the ^{13}C NMR spectrum of man-Azo-P1. Together, these assigned signals provide direct evidence for the successful construction of the azo polymers from their corresponding monomers. The FT-IR spectra provide additional structure elucidation for the azo-linkage formation between the diamine and the 1,3,5-trihydroxybenzene (Figure 1b,c). The vibrational band around 1400 cm^{-1} confirms the presence of the azo (−N═N−) group.[23,26] On the other hand, the disappearance of the NH_2 bands of the monomers (two sharp bands around 3400 cm^{-1}) in the resulting polymers is also direct evidence of the azo coupling formation of the diamine monomers. In comparison, the broad band centered at 3404 cm^{-1} in the polymers is attributed to the 1,3,5-trihydroxy monomer in the structure. The powder X-ray diffraction analysis of the synthesized Azo-man-P1 and Azo-man-P2 has demonstrated the amorphous nature of both materials with a broad peak centered at around 20°, as shown in Figure S3. The SEM images show the amorphous microstructures of the samplse with irregular shapes (Figures S4 and S6). A TGA study and DSC analysis proved the thermal stability of the polymers and (Figures S1 and S2). The first decomposition after the solvent removal started at around 300 °C for man-Azo-P1 and at around 250 °C for man-Azo-P2.

https://doi.org/10.1021/acsomega.1c05905
ACS Omega 2022, 7, 14535−14543

Porosity and Pore Structure. After structure characterization of the synthesized azo-linked polymers, the permanent porosity of the materials was investigated by measuring the adsorption−desorption nitrogen isotherms at 77 K (Figure 2a). The N_2 isotherms reveal high uptake at the low-pressure region ($P/P^0 < 0.001$) for both man-Azo-P1 and man-Azo-P2, indicating the presence of micropores within the frameworks. The higher uptake at the higher pressure ($P/P^0 < 0.5$) is due to the capillary condensation of the N_2 in the meso- and macropore behavior. The pore size distribution (PSD) was estimated using quenched solid density functional theory (QSDFT) model which quantitively represents the surface geometrical inhomogeneity in terms of roughness parameters, including micro-/mesopore structures. The PSD proves that man-Azo-P1 is mainly a micropore material while man-Azo-P2 has both micropore and mesopore textures (Figure 2b) that may be attributed to the flexibility of the 4,4′-methylenedianiline monomers of the azo-man-P2 framework. The calculated Brunauer−Emmitt-Teller (BET) surface aresa of man-Azo-P1 and man-Azo-P2 were found to be 290 and 78 $m^2\ g^{-1}$, respectively. The BET surface areas, and pore volumes, and diameters are summarized in Table 1.

Table 1. Surface Areas and Pore Parameters of the Synthesized man-Azo-P1 and man-Azo-P2 Materials

sample	BET surface area ($m^2\ g^{-1}$)	Langmuir surface area ($m^2\ g^{-1}$)	PSD[a] (nm)	pore volume ($cm^3\ g^{-1}$)[c]
man-Azo-P1	290	450	0.3	0.33
man-Azo-P2	78	123	59.6	0.15

[a]PSD calculated by the QSDFT model. [c]DFT accumulated pore volume.

CO_2 Gas Uptake Measurements. Inspired by the intrinsic microporosity of the developed man-Azo-P1 and man-Azo-P2 materials and the subunit core polar functionality of the frameworks, we were encouraged to investigate the CO_2 adsorption capabilities. The thermodynamic adsorption measurements for CO_2 and N_2 were assessed at two different temperatures (273 and 298 K) to evaluate the capacity of man-Azo-P1 and man-Azo-P2 toward CO_2 capture. As shown in Figure 3a, man-Azo-P1 has a high uptake capacity in comparison to man-Azo-P2, although they have similar functionalities. However, this is due to the difference in the surface area. The steep high CO_2 uptake and low pressure for both materials in comparison to the poor uptake for N_2 indicate the strong affinity of the synthesized azo polymers toward the CO_2 thanks to the CO_2-philic functional groups (−N═N− and OH) in the frameworks. The CO_2 uptake capacities were found to be 32 and 20 $cm^3\ g^{-1}$ at 273 K and 1 bar for man-Azo-P1 and man-Azo-P2, respectively, in comparison with only 1.4 and 1.4 $cm^3\ g^{-1}$ at 273 K and 1 bar for the N_2 uptake. It is worth mentioning the high affinity of man-Azo-P1 toward CO_2 in comparison to the low CO_2 uptake for man-Azo-P2. In contrast, similar uptake capacities for N_2 indicate the crucial role of the high surface area and microporosity in addition to the polar functionality. The CO_2 uptake capacity of man-Azo-P1 is comparable with those of previously reported porous organic polymers at 273 K and 1 bar. These include the crystalline covalent organic frameworks; (COF-5, 29.9 $cm^3\ g^{-1}$; COF, 8:32 $cm^3\ g^{-1}$; COF-10, 27.0 $cm^3\ g^{-1}$).[27] However, the uptake is lower than for other amine cross-linked polymers due to the lower surface area (PTPM-1 38.6 $cm^3\ g^{-1}$, mPTPM-1 43.3 $cm^3\ g^{-1}$;[28] NCMPs 56.0 $cm^3\ g^{-1}$;[29] polycarbazole network PCZNs 38.1−71.2 $cm^3\ g^{-1}$;[30] HCMP-1 38 $cm^3\ g^{-1}$)[31] and other Azo-POPs with similar functionalities such as Azo-COPs (22.4−33.6 $cm^3\ g^{-1}$)[32] and triptycene azo polymers (TAP-1 48.4 $cm^3\ g^{-1}$, TAP-2 71.8 $cm^3\ g^{-1}$).[23]

Coverage-Dependent Enthalpy of Adsorption and CO_2/N_2 Selectivity. Encouraged by the good thermodynamic CO_2 uptake of the synthesized azo-linked polymers and a further understanding of the interaction of the man-Azo-P1 and man-Azo-P2 with the adsorbed CO_2 molecules, we calculated the coverage-dependent enthalpy of adsorption (Q_{st}). The Q_{st} values were estimated by fitting the CO_2 and N_2 isotherms at 273 and 298 K using a viral type expansion equation (eq S1 in the Supporting Information). The initial Q_{st} values (at zero coverage) for man-Azo-P1 and man-Azo-P2 for CO_2 were 40 and 23 kJ mol^{-1}, respectively, in comparison to only 4.4 and 22.0 kJ mol^{-1} for N_2, indicating the strong binding of CO_2 with the polymer frameworks. These Q_{st} values are high enough for favorable physical adsorption of CO_2 but are still not very high, as for the aliphatic amine-based sorbents in which the strong binding with CO_2 forming a carbamate needs high energy for regeneration.[18,33,34] The CO_2/N_2 selectivity was estimated using the ideal adsorption solution theory (IAST) model. As such, man-Azo-P1 showed a good CO_2/N_2 selectivity of about 80 at 1 bar and 273 K (Figure 3c).

Metal Ion Removal Application. The prepared polymers man-Azo-P1 and man-Azo-P2 were evaluated for their efficiency in the adsorption of metal ions from aqueous media. As shown in Figure 4, the results indicated that both polymers have high efficiency toward the adsorption of the metal ions. However, man-Azo-P1 showed slightly better performance compared with man-Azo-P2, which can be explained by its higher surface area and porous structure. In addition, the possible mechanisms of interactions include the formation of complexes, surface complexation, π−metal interactions, and interactions with functional groups, as well as electrostatic interactions.[35−37] As it showed better performance, man-Azo-P1 was selected for further investigation. The prepared polymer man-Azo-P1 was evaluated with regard to the contact time effect on the adsorption of metal ions from aqueous media.

To get insights into the capacity of polymers for metal adsorption, the capacity was presented in milligrams of the metal per gram of polymer, as shown in Figure 5. The capacity of adsorption of metal ions increased with the increase of contact time. At contact times of around 90 and 120 min, the adsorption was almost constant, indicating an equilibrium.

The effect of man-Azo-P1 dosage was investigated as in Figure 6a. By an increase in the dosage, the adsorption increased; this can be explained by the presence of more surface area and active functional groups to interact with the metal ions. The effect of the pH of the solution was also studied in the range between 3 and 7. It can be seen in Figure 6b that, by increasing the pH, the removal of metal ions increased. At pH 3, the removal was low, which can be explained by the presence of more protons that compete with the positively charged metal ions.[38] At higher pH, there are fewer protons and most partially negatively charged functional groups are ready to interact with the metal ions. The presence

https://doi.org/10.1021/acsomega.1c05905
ACS Omega 2022, 7, 14535−14543

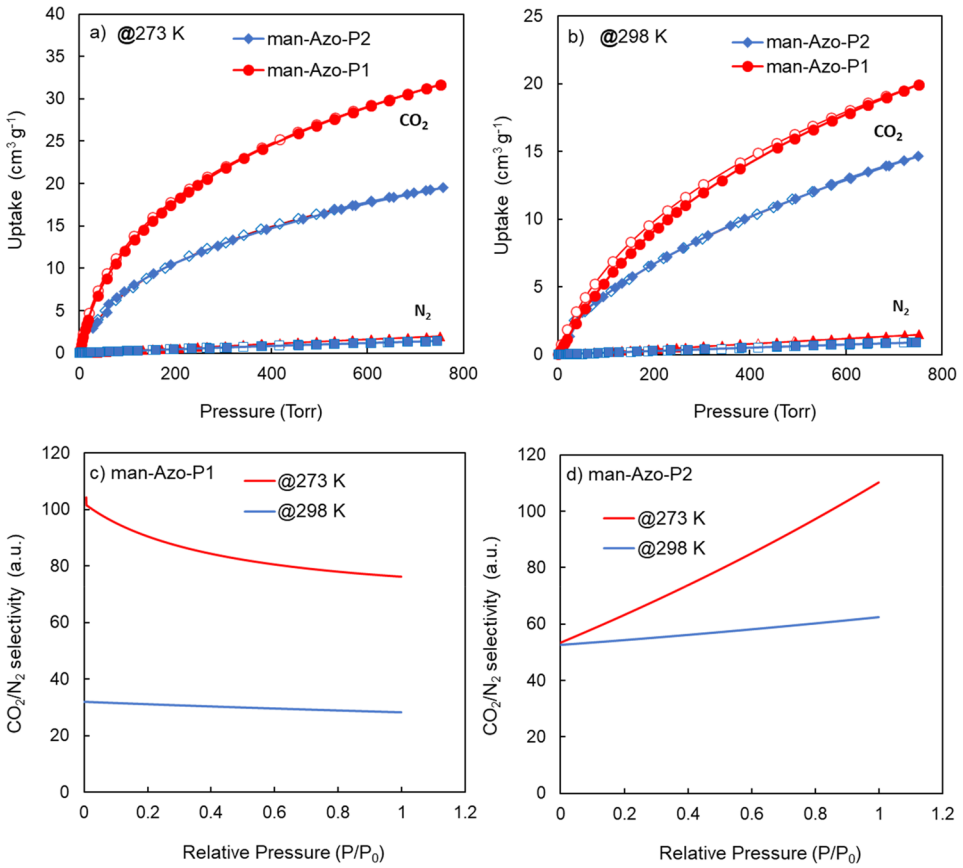

Figure 3. Gas sorption analysis of man-Azo-P1 (red, circles) and man-Azo-P2 (blue, rhombohedrons) at 273 K (a) and 298 K (b). Ideal adsorption solution theory (IAST) CO_2/N_2 selectivity at 273 K (red) and 298 K (blue) of man-Azo-P1 (c) and man-Azo-P2 (d).

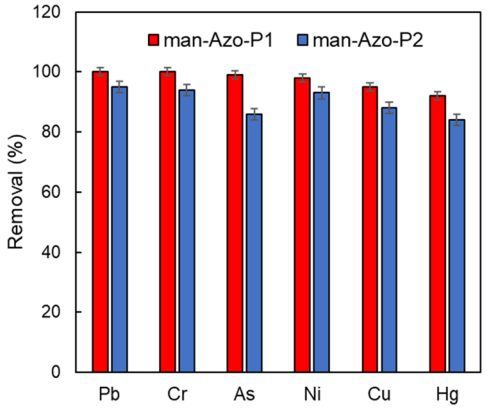

Figure 4. Adsorption efficiencies of (i) man-Azo-P1 (red) and (ii) man-Azo-P2 (blue) for the simultaneous removal of metal ions. Conditions: initial concentration 100 ppm, contact time 120 min, pH 6, and dosage of 25 mg/20 mL.

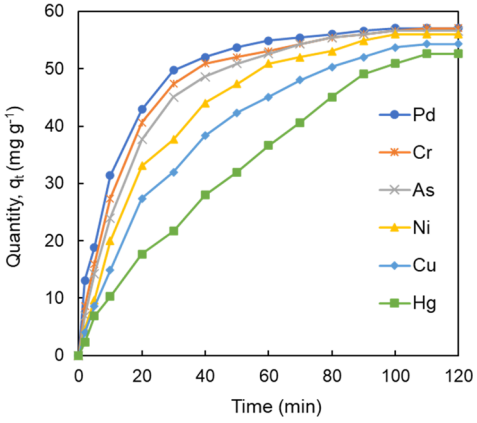

Figure 5. Effect of contact time on the efficiency of the polymer man-Azo-P1 for the removal of metal ions: lead (dark blue), chromium (orange), arsenic (gray), nickel (yellow), copper (light blue), and mercury (green).

of nonbonding electrons on oxygen and nitrogen also plays a significant role in interacting with negatively charged metal ions.[39] These results highlight the high removal performance of the synthesized azo-polymerscomparable with those reported in the literature.[40,41] man-Azo-P1 showed promising recycling performance for removing metals even after five cycles of adsorption/desorption (Figure 7). The excellent performance of the reported polymers indicates that they can be used several times due to their easy regeneration. Therefore, the reported polymers can be recommended for water treatment. The highest capacity was for the removal of lead, chromium, and arsenic, followed by nickel, copper, and mercury, which showed slightly less capacity.

CONCLUSION

In conclusion, the synthesis and scale-up of two azo-linked polymers denoted man-Azo-P1 and man-Azo-P2 were achieved in water as a solvent at low temperature (0 °C) via diazotization of 4,4′-diaminobiphenyl (benzidine) and 4,4′-diaminodianiline with phloroglucinol. The synthesized man-Azo-P1 polymer showed a good BET surface area of 290 m^2

https://doi.org/10.1021/acsomega.1c05905
ACS Omega 2022, 7, 14535−14543

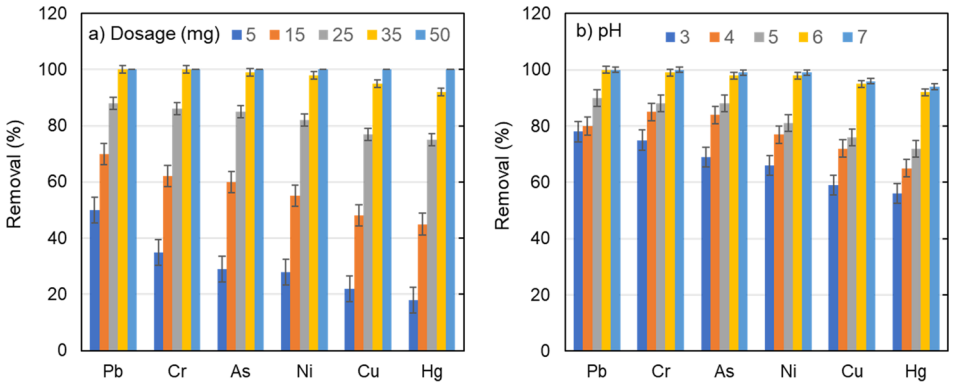

Figure 6. (a) Effect of polymer P2 dosage of (i) 5, (ii) 15, (iii) 25, (iv) 35, and (v) 50 mg/20 mL, on the removal of metal ions. Conditions: contact time 120 min and pH 6. (b) Effect of pH (3, 4, 5, 6, and 7) on the efficiency of the polymer P1 for the removal of metal ions. Condition: contact time 120 min.

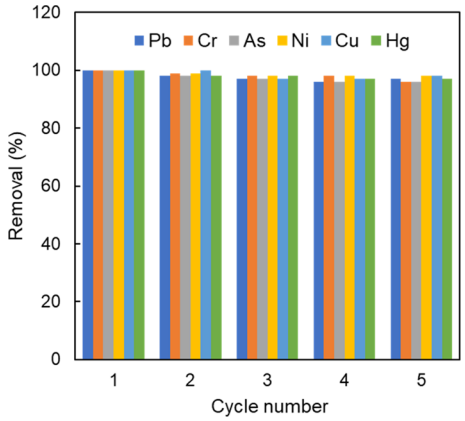

Figure 7. Excellent performance of man -Azo-P1 for metal removal over five cycles. Conditions: dosage 50 mg, pH 6, and time 120 min.

g^{-1}, which is higher than that of man-Azo-P2 of 78 m^2 g^{-1} that was attributed to the role of the rigidity of the starting 4,4′-diaminobiphenyl monomer in comparison to the flexible 4,4′-methylenedianiline. The man-Azo-P1 material showed good CO_2 uptake, due to the good surface area and the polar azo and hydroxy functional groups decorating the porous structure. Additionally, the synthesized materials were explored for the removal of toxic metal ions from water. Both materials showed high capabilities for removing different metal ions with 100% removal for Cr and Pb. Such results demonstrate the great potential of the synthesized azo-linked POPs for environmental application.

■ ASSOCIATED CONTENT

Supporting Information

The Supporting Information is available free of charge at https://pubs.acs.org/doi/10.1021/acsomega.1c05905.

TGA and additional selectivity calculations (PDF)

■ AUTHOR INFORMATION

Corresponding Author

Mahmoud M. Abdelnaby − *Interdisciplinary Research Center for Hydrogen and Energy Storage (IRC-HES), King Fahd University of Petroleum and Minerals (KFUPM), Dhahran 31261, Saudi Arabia;* orcid.org/0000-0003-3434-8593; Email: mahmoudm@kfupm.edu.sa

Authors

Tawfik A. Saleh − *Department of Chemistry, King Fahd University of Petroleum and Minerals (KFUPM), Dhahran 31261, Saudi Arabia*

Mostafa Zeama − *Interdisciplinary Research Center for Hydrogen and Energy Storage (IRC-HES), King Fahd University of Petroleum and Minerals (KFUPM), Dhahran 31261, Saudi Arabia*

Mahmoud Atef Abdalla − *Interdisciplinary Research Center for Hydrogen and Energy Storage (IRC-HES), King Fahd University of Petroleum and Minerals (KFUPM), Dhahran 31261, Saudi Arabia*

Hossam M. Ahmed − *Interdisciplinary Research Center for Hydrogen and Energy Storage (IRC-HES), King Fahd University of Petroleum and Minerals (KFUPM), Dhahran 31261, Saudi Arabia*

Mohamed A. Habib − *Mechanical Engineering Department, Faculty of Engineering, KFUPM, Dhahran 31261, Saudi Arabia; KA CARE Energy Research & Innovation Center at Dhahran, Dhahran 31261, Saudi Arabia;* orcid.org/0000-0003-3459-1462

Complete contact information is available at: https://pubs.acs.org/10.1021/acsomega.1c05905

Author Contributions

The manuscript was written through the contributions of all authors./All authors have approved the final version of the manuscript.

Notes

The authors declare no competing financial interest.

■ ACKNOWLEDGMENTS

The authors acknowledge the support provided by the Deanship of the Research Oversight and Coordination (DROC) at King Fahd University of Petroleum and Minerals (KFUPM) for funding this work through project no. DF201009.

■ REFERENCES

(1) Cheung, O.; Hedin, N. Zeolites and related sorbents with narrow pores for CO_2 separation from flue gas. *RSC Adv.* **2014**, *4* (28), 14480−14494.

(2) Trickett, C. A.; Helal, A.; Al-Maythalony, B. A.; Yamani, Z. H.; Cordova, K. E.; Yaghi, O. M. The chemistry of metal−organic

frameworks for CO_2 capture, regeneration and conversion. *Nat. Rev. Mater.* **2017**, *2* (8), 17045.
(3) Zeng, Y.; Zou, R.; Zhao, Y. Covalent Organic Frameworks for CO2 Capture. *Adv. Mater.* **2016**, *28* (15), 2855−2873.
(4) Wang, L.; Guo, J.; Xiang, X.; Sang, Y.; Huang, J. Melamine-supported porous organic polymers for efficient CO_2 capture and Hg2+ removal. *Chem. Eng. J.* **2020**, *387*, 124070.
(5) Chen, Q.; Tan, X.; Liu, Y.; Liu, S.; Li, M.; Gu, Y.; Zhang, P.; Ye, S.; Yang, Z.; Yang, Y. Biomass-derived porous graphitic carbon materials for energy and environmental applications. *J. Mater. Chem. A* **2020**, *8* (12), 5773−5811.
(6) Tian, W.; Zhang, H.; Duan, X.; Sun, H.; Shao, G.; Wang, S. Porous Carbons: Structure-Oriented Design and Versatile Applications. *Adv. Funct. Mater.* **2020**, *30* (17), 1909265.
(7) Lv, B.; Guo, B.; Zhou, Z.; Jing, G. Mechanisms of CO2 Capture into Monoethanolamine Solution with Different CO2 Loading during the Absorption/Desorption Processes. *Environ. Sci. Technol.* **2015**, *49* (17), 10728−10735.
(8) Wu, X.; Cobbina, S. J.; Mao, G.; Xu, H.; Zhang, Z.; Yang, L. A review of toxicity and mechanisms of individual and mixtures of heavy metals in the environment. *Environ. Sci. Pollut. Res.* **2016**, *23* (9), 8244−8259.
(9) Ozdemir, J.; Mosleh, I.; Abolhassani, M.; Greenlee, L. F.; Beitle, R. R.; Beyzavi, M. H. Covalent Organic Frameworks for the Capture, Fixation, or Reduction of CO_2. *Front. Energy Res.* **2019**, *7* (77), 1.
(10) Dey, S.; Bhunia, A.; Esquivel, D.; Janiak, C. Covalent triazine-based frameworks (CTFs) from triptycene and fluorene motifs for CO_2 adsorption. *J. Mater. Chem. A* **2016**, *4* (17), 6259−6263.
(11) Hug, S.; Stegbauer, L.; Oh, H.; Hirscher, M.; Lotsch, B. V. Nitrogen-Rich Covalent Triazine Frameworks as High-Performance Platforms for Selective Carbon Capture and Storage. *Chem. Mater.* **2015**, *27* (23), 8001−8010.
(12) Díaz, U.; Corma, A. Ordered covalent organic frameworks, COFs and PAFs. From preparation to application. *Coord. Chem. Rev.* **2016**, *311*, 85−124.
(13) Xu, Y.; Jin, S.; Xu, H.; Nagai, A.; Jiang, D. Conjugated microporous polymers: design, synthesis and application. *Chem. Soc. Rev.* **2013**, *42* (20), 8012−8031.
(14) Xie, Y.; Wang, T.-T.; Liu, X.-H.; Zou, K.; Deng, W.-Q. Capture and conversion of CO_2 at ambient conditions by a conjugated microporous polymer. *Nat. Commun.* **2013**, *4* (1), 1960.
(15) Yang, L.; Tian, Z.; Zhang, X.; Wu, X.; Wu, Y.; Wang, Y.; Peng, D.; Wang, S.; Wu, H.; Jiang, Z. Enhanced CO2 selectivities by incorporating CO_2-philic PEG-POSS into polymers of intrinsic microporosity membrane. *J. Membr. Sci.* **2017**, *543*, 69−78.
(16) Elmehalmey, W. A.; Azzam, R. A.; Hassan, Y. S.; Alkordi, M. H.; Madkour, T. M. Imide-Based Polymers of Intrinsic Microporosity: Probing the Microstructure in Relation to CO_2 Sorption Characteristics. *ACS Omega* **2018**, *3* (3), 2757−2764.
(17) Abdelnaby, M. M.; Alloush, A. M.; Qasem, N. A. A.; Al-Maythalony, B. A.; Mansour, R. B.; Cordova, K. E.; Al Hamouz, O. C. S. Carbon dioxide capture in the presence of water by an amine-based crosslinked porous polymer. *J. Mater. Chem. A* **2018**, *6* (15), 6455−6462.
(18) Abdelnaby, M. M.; Qasem, N. A. A.; Al-Maythalony, B. A.; Cordova, K. E.; Al Hamouz, O. C. S. A Microporous Organic Copolymer for Selective CO2 Capture under Humid Conditions. *ACS Sustainable Chem. Eng.* **2019**, *7* (16), 13941−13948.
(19) Tan, L.; Tan, B. Hypercrosslinked porous polymer materials: design, synthesis, and applications. *Chem. Soc. Rev.* **2017**, *46* (11), 3322−3356.
(20) Patel, H. A.; Je, S. H.; Park, J.; Jung, Y.; Coskun, A.; Yavuz, C. T. Directing the Structural Features of N_2-Phobic Nanoporous Covalent Organic Polymers for CO_2 Capture and Separation. *Chem. - Eur. J.* **2014**, *20* (3), 772−780.
(21) El-Kadri, O. M.; Tessema, T.-D.; Almotawa, R. M.; Arvapally, R. K.; Al-Sayah, M. H.; Omary, M. A.; El-Kaderi, H. M. Pyrene Bearing Azo-Functionalized Porous Nanofibers for CO_2 Separation and Toxic Metal Cation Sensing. *ACS Omega* **2018**, *3* (11), 15510−15518.
(22) Liu, M.; Yao, C.; Liu, C.; Xu, Y. Ag+ doped into azo-linked conjugated microporous polymer for volatile iodine capture and detection of heavy metal ions. *Sci. Rep.* **2018**, *8* (1), 14072.
(23) Bera, R.; Ansari, M.; Alam, A.; Das, N. Triptycene, Phenolic-OH, and Azo-Functionalized Porous Organic Polymers: Efficient and Selective CO_2 Capture. *ACS Appl. Polym. Mater.* **2019**, *1* (5), 959−968.
(24) Liaw, D.-J.; Chang, F.-C.; Leung, M.-k.; Chou, M.-Y.; Muellen, K. High Thermal Stability and Rigid Rod of Novel Organosoluble Polyimides and Polyamides Based on Bulky and Noncoplanar Naphthalene−Biphenyldiamine. *Macromolecules* **2005**, *38* (9), 4024−4029.
(25) Liu, X.; Luo, X.-S.; Deng, H.-L.; Fan, W.; Wang, S.; Yang, C.; Sun, X.-Y.; Chen, S.-L.; Huang, M.-H. Functional Porous Organic Polymers Comprising a Triaminotriphenylazobenzene Subunit as a Platform for Copper-Catalyzed Aerobic C−H Oxidation. *Chem. Mater.* **2019**, *31* (15), 5421−5430.
(26) Ji, G.; Yang, Z.; Zhang, H.; Zhao, Y.; Yu, B.; Ma, Z.; Liu, Z. Hierarchically Mesoporous o-Hydroxyazobenzene Polymers: Synthesis and Their Applications in CO2 Capture and Conversion. *Angew. Chem., Int. Ed.* **2016**, *55* (33), 9685−9689.
(27) Furukawa, H.; Yaghi, O. M. Storage of Hydrogen, Methane, and Carbon Dioxide in Highly Porous Covalent Organic Frameworks for Clean Energy Applications. *J. Am. Chem. Soc.* **2009**, *131* (25), 8875−8883.
(28) Hu, X.; Wang, H.; Faul, C. F. J.; Wen, J.; Wei, Y.; Zhu, M.; Liao, Y. A crosslinking alkylation strategy to construct nitrogen-enriched tetraphenylmethane-based porous organic polymers as efficient carbon dioxide and iodine adsorbents. *Chem. Eng. J.* **2020**, *382*, 122998.
(29) Liao, Y.; Cheng, Z.; Zuo, W.; Thomas, A.; Faul, C. F. J. Nitrogen-Rich Conjugated Microporous Polymers: Facile Synthesis, Efficient Gas Storage, and Heterogeneous Catalysis. *ACS Appl. Mater. Interfaces* **2017**, *9* (44), 38390−38400.
(30) Liao, Y.; Cheng, Z.; Trunk, M.; Thomas, A. Targeted control over the porosities and functionalities of conjugated microporous polycarbazole networks for CO_2-selective capture and H_2 storage. *Polym. Chem.* **2017**, *8* (46), 7240−7247.
(31) Liao, Y.; Weber, J.; Mills, B. M.; Ren, Z.; Faul, C. F. J. Highly Efficient and Reversible Iodine Capture in Hexaphenylbenzene-Based Conjugated Microporous Polymers. *Macromolecules* **2016**, *49* (17), 6322−6333.
(32) Patel, H. A.; Hyun Je, S.; Park, J.; Chen, D. P.; Jung, Y.; Yavuz, C. T.; Coskun, A. Unprecedented high-temperature CO2 selectivity in N_2-phobic nanoporous covalent organic polymers. *Nat. Commun.* **2013**, *4* (1), 1357.
(33) Nugent, P.; Belmabkhout, Y.; Burd, S. D.; Cairns, A. J.; Luebke, R.; Forrest, K.; Pham, T.; Ma, S.; Space, B.; Wojtas, L.; Eddaoudi, M.; Zaworotko, M. J. Porous materials with optimal adsorption thermodynamics and kinetics for CO_2 separation. *Nature* **2013**, *495* (7439), 80−84.
(34) Abdelnaby, M. M.; Cordova, K. E.; Abdulazeez, I.; Alloush, A. M.; Al-Maythalony, B. A.; Mankour, Y.; Alhooshani, K.; Saleh, T. A.; Al Hamouz, O. C. S. Novel Porous Organic Polymer for the Concurrent and Selective Removal of Hydrogen Sulfide and Carbon Dioxide from Natural Gas Streams. *ACS Appl. Mater. Interfaces* **2020**, *12* (42), 47984−47992.
(35) Swiatkowski, A.; Pakula, M.; Biniak, S.; Walczyk, M. Influence of the surface chemistry of modified activated carbon on its electrochemical behaviour in the presence of lead(II) ions. *Carbon* **2004**, *42* (15), 3057−3069.
(36) Zhang, L.; Pan, F.; Liu, X.; Yang, L.; Jiang, X.; Yang, J.; Shi, W. Multi-walled carbon nanotubes as sorbent for recovery of endocrine disrupting compound-bisphenol F from wastewater. *Chem. Eng. J.* **2013**, *218*, 238−246.

https://doi.org/10.1021/acsomega.1c05905
ACS Omega 2022, 7, 14535−14543

(37) Aksu, Z.; Akın, A. B. Comparison of Remazol Black B biosorptive properties of live and treated activated sludge. *Chem. Eng. J.* **2010**, *165* (1), 184−193.
(38) Shariful, M. I.; Sepehr, T.; Mehrali, M.; Ang, B. C.; Amalina, M. A. Adsorption capability of heavy metals by chitosan/poly(ethylene oxide)/activated carbon electrospun nanofibrous membrane. *J. Appl. Polym. Sci.* **2018**, *135* (7), 45851.
(39) Chen, G.; Liu, Y.; Liu, F.; Zhang, X. Fabrication of three-dimensional graphene foam with high electrical conductivity and large adsorption capability. *Appl. Surf. Sci.* **2014**, *311*, 808−815.
(40) Huang, S.; Ma, C.; Liao, Y.; Min, C.; Du, P.; Zhu, Y.; Jiang, Y. Superb adsorption capacity and mechanism of poly(1-amino-5-chloroanthraquinone) nanofibrils for lead and trivalent chromium ions. *React. Funct. Polym.* **2016**, *106*, 76−85.
(41) Liao, Y.; Cai, S.; Huang, S.; Wang, X.; Faul, C. F. J. Macrocyclic Amine-Linked Oligocarbazole Hollow Microspheres: Facile Synthesis and Efficient Lead Sorbents. *Macromol. Rapid Commun.* **2014**, *35* (21), 1833−1839.

https://doi.org/10.1021/acsomega.1c05905
ACS Omega 2022, 7, 14535−14543